

# DRL-ISP: Multi-Objective Camera ISP with Deep Reinforcement Learning

Ukcheol Shin\*, Kyunghyun Lee\*, and In So Kweon

**Abstract**—In this paper, we propose a multi-objective camera ISP framework that utilizes Deep Reinforcement Learning (DRL) and camera ISP toolbox that consist of network-based and conventional ISP tools. The proposed DRL-based camera ISP framework iteratively selects a proper tool from the toolbox and applies it to the image to maximize a given vision task-specific reward function. For this purpose, we implement total 51 ISP tools that include exposure correction, color-and-tone correction, white balance, sharpening, denoising, and the others. We also propose an efficient DRL network architecture that can extract the various aspects of an image and make a rigid mapping relationship between images and a large number of actions. Our proposed DRL-based ISP framework effectively improves the image quality according to each vision task such as RAW-to-RGB image restoration, 2D object detection, and monocular depth estimation.

## I. INTRODUCTION

In recent years, the importance of vision sensors has been re-emphasized as deep learning has demonstrated superior performance in various computer vision tasks. Despite the importance, visible-light cameras suffer from hardware limitations such as narrow dynamic range and low sensor sensitivity. For this problem, the conventional camera performs a built-in Image Signal Processing (ISP) that improves image quality by applying sequential modifications such as de-blurring, de-noising, and color enhancement. However, the built-in ISP usually consists of a fixed image processing pipeline with factory-tuned hyperparameters. Therefore, the built-in ISP usually does not guarantee an optimal quality image for various computer vision tasks.

On the other hands, recent deep-learning based approaches shows notable results such as direct RAW-to-RGB recovery [1], [2], denoising [3], super resolution [4], [5], white-balance [6], [7], tone-mapping [8], [9], and exposure correction [10], [11], [12] through a single deep neural network. However, they require high computational costs and can only replace a specific part of the camera ISP pipeline.

Based on the observation, we propose a new camera ISP framework that utilizes Deep Reinforcement Learning (DRL) and camera ISP toolbox that includes both traditional image processing tools and network-based tools. Our DRL framework applies the most appropriate ISP tools based on the current image state to maximize a target reward function with a given demosaiced RAW image. Based on designed reward functions, the DRL agent can generate an image

\*Both authors contributed equally to this work.

This work was conducted by Center for Applied Research in Artificial Intelligence (CARAI) grant funded by DAPA and ADD (UD190031RD).

U. Shin, K. Lee, and I. S. Kweon are with the School of Electrical Engineering, KAIST, Daejeon 34141, Republic of Korea. {shinwc159, kyunghyun.lee, iskweon77}@kaist.ac.kr

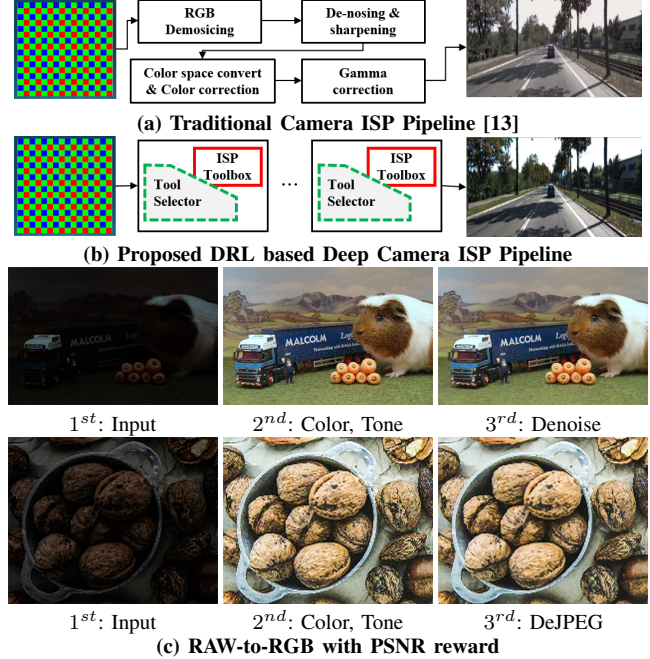


Fig. 1. **Overview of the proposed DRL-based Camera ISP framework.** The traditional camera ISP framework (a) usually consists of a non-flexible image processing pipeline with factory-tuned hyperparameters. On the other hand, the proposed DRL-based ISP framework (b) has a flexible pipeline that can adaptively process a given image by selecting desirable ISP tools sequentially (c).

suitable for various tasks, such as general RAW-to-RGB recovery, object detection, and depth estimation.

Our contributions include the following:

- We propose a novel DRL-based camera ISP framework that effectively performs a suitable action according to the current image state and target reward function.
- We propose a camera ISP toolbox along with its training method. The toolbox consists of light-weight CNN tools and traditional tools that can represent each block of the camera ISP pipeline.
- We propose an efficient DRL network architecture that extracts various aspects of an image and build rigid mapping relationships between images and a large number of action space.
- We validate our proposed method for RAW-to-RGB image restoration, 2D object detection, and monocular depth estimation tasks. The proposed method consecutively increases the performance of the target task by modifying images suitably.

## II. RELATED WORK

### A. Camera ISP Parameter Optimization

Traditionally, the RGB image is recovered from the RAW image through a camera built-in ISP chipset that consists of various image processing blocks. Recently, several approaches have explored the automatic camera ISP optimization with various objectives [14], [15], [16], [17], [18], [19], [20]. Each image processing block of the ISP chipset is usually a black-box. Therefore, some researches optimize chipset’s hyperparameters through black-box optimization [14], evolutionary algorithm [18], and reinforcement learning [19]. Other approaches [17], [15] parameterize the operation of each block or entire ISP pipeline as a neural network. After that, they optimize the hyperparameter through the approximated neural network.

Sometimes, they optimize hyperparameters for low-level image enhancement [17], [15], object detection [16], human preference [20], and high-level scene understanding [21], [19]. However, Their methods rely on a fixed ISP pipeline and hyperparameters. Therefore, they cannot easily add a new image processing module and change the parameters according to a new image or new environment adaptively.

### B. Learning Camera ISP Pipeline

Recently, neural network based approaches [22], [1], [2], [23], [24] are emerging to directly recover a high-quality RGB image from RAW sensory data through a single deep neural network. Their underlying idea is to embed the entire ISP pipeline, including demosaicing, denoising, sharpening, color correction, and white balance, into a single deep neural network. Mainly, their objective is well-exposed images [2], [22], expert retouched images [23], and well-captured camera images [1], [24].

Contrarily, some studies have been proposed to approximate only a specific part of the ISP pipeline, such as white-balance [6], [7], tone-mapping [8], [9], and exposure correction [10], [11], [12]. These entire and partial replacements show higher performance than typical ISP pipelines and specific modules. However, the networks are usually computationally heavy and impossible to specialize for non-differentiable objectives (*e.g.* well-exposed and edge-preserving image, object detection, or high-level scene understanding).

## III. METHOD OVERVIEW

### A. Problem Definition

We treat the camera ISP pipeline as a *sequential decision making problem* that iteratively decides proper action  $a_t$  according to the current image state  $s_t$ . Given a demosaiced RAW image, our goal is to make an enhanced optimal image  $I_{opt}$  for a target reward function  $R(\cdot)$ . We define each Image Signal Processing (ISP) tool as an action  $a_t$ , image feature  $f^{ag}$  extracted from the demosaiced RAW image as a state  $s_t$ , and target-task specific objective function as a reward function  $R(\cdot)$ .

TABLE I

CAMERA ISP TOOLBOX SPECIFICATION. THE ISP TOOLBOX CONSISTS OF BOTH TRADITIONAL AND NETWORK-BASED IMAGE PROCESSING TOOLS. THE NUMBER OF (·) INDICATES EACH TOOL HAS THE CORRESPONDING NUMBER OF ACTIONS.

Type	Network-based Tools	Traditional Tools
Brightness	ExposureNet (x2)	Brightness modification (x12)
Contrast	CTCNet (x2)	Histogram equalization, CLAHE [26], Gamma correction (x6)
Color	WBNet (x2)	Hue modification (x6), Saturation modification (x6), White Balance [27]
Noise	DenoiseNet (x2)	Gaussian, box, bilateral filter
Blur	DeblurNet (x2)	Sharpening filter
Others	SRNet (x2) DejpgNet (x2)	Do nothing

### B. Camera ISP Toolbox

The proposed framework consists of camera ISP toolbox and tool selector, as shown in Fig. 2 and Tab. I. We design the toolbox to include the functionality of each camera ISP module, such as white balance, denoising, sharpening, and color-and-tone correction. The proposed toolbox exploits traditional and learning-based methods to leverages both high performances of the deep network and controllability of the traditional tools. All network based tools are trained in a self-supervised manner.

### C. DRL-based ISP Tool Selector

The tool selector consists of a feature extractor and Deep Reinforcement Learning (DRL) agent. The feature extractor extracts representative feature vector  $f^{ag}$  that consists of intensity, gradient, and semantic information. After that, the DRL agent chooses a proper ISP tool to maximize the target reward function. The DRL agent is trained with the policy gradient algorithm, proposed in [25].

## IV. CAMERA ISP TOOLBOX

The CNN-based tools show a high-representation capacity that encompasses complicated multi-step image processing pipeline while showing outperformed results. However, they usually produce one-way mapping results, are non-controllable to get another result, and sometimes lead to undesirable results. On the other hand, even though traditional tools do not perform better than the CNN tools, traditional image processing tools have been already demonstrated their computational efficiency, stability, and controllability. Therefore, we design the camera ISP toolbox to include both traditional and learning-based tools for performance, stability, and controllability, as shown in Tab. I.

### A. Traditional ISP Tools

We implement brightness, contrast, color, noise, and blur handling methods from the openCV [28] and Korina library [29]. We consider this implementation can prop-

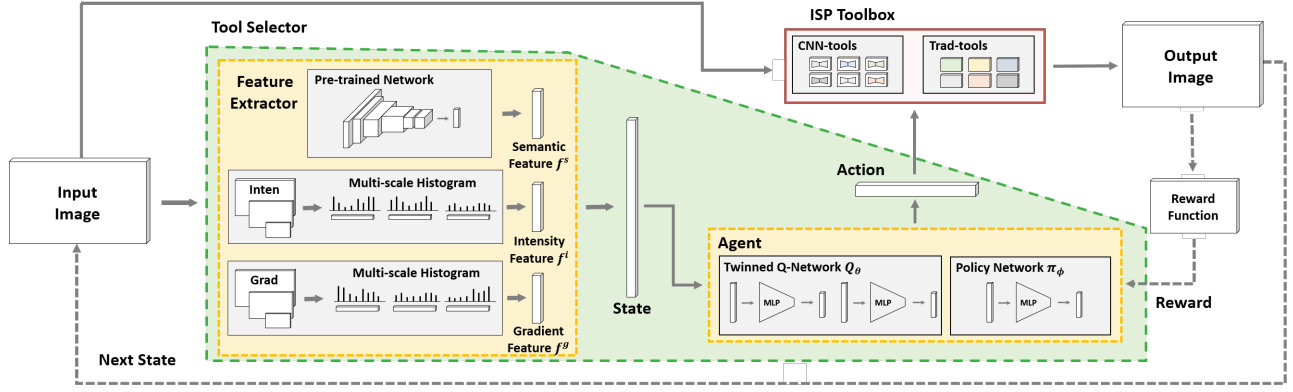


Fig. 2. **Overall pipeline of the proposed DRP-ISP framework.** The proposed DRL-ISP framework consists of a feature extractor  $F$  and camera ISP toolbox. The ISP toolbox exploits both CNN-based and traditional image processing tools that can represent each block of the camera ISP pipeline. With a given image input, the feature extractor  $F$  extracts an efficient feature vector  $f^{ag}$  that includes intensity, gradient, and semantic information. The policy network  $\pi_\phi$  selects optimal action according to the feature vector  $f^{ag}$  to maximize a target reward function. The twinned Q-networks  $Q_\theta$  are only utilized during the training.

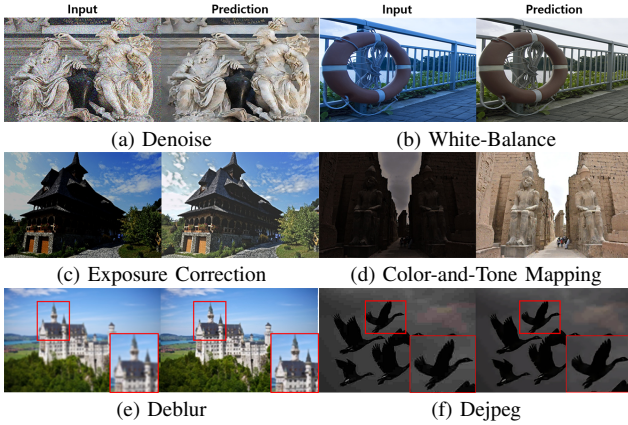


Fig. 3. **Qualitative results of each CNN-based ISP tool.** Each CNN tool is trained to solve each target task, such as denoise, deblur, exposure correction, color mapping, and white balance, in a self-supervised manner.

erly represents each block of camera ISP such as white-balance, denoising, sharpening, and color correction. The same philosophy is incorporated into network-based tool designing, such as exposure correction, Color-and-Tone Correction(CTC), White-Balance(WB), denoise, deblur, Super-Resolution(SR), and de-jpeg network.

## B. Learning-based ISP Tools

1) *Individual Tool Training.*: In order to make light-weight network-based ISP tools, we adopt shallow 3-layer and 8-layer neural networks proposed in [30]. We train each network in a self-supervised learning manner for each target task. Given an original image  $I_{ori}$ , we make a distorted image  $I_{dis}$  according to the target network tool type. For example, if we want to train the de-blur network, we apply blur kernel to the original image and make a distorted image. After that, we train the networks to restore the original image  $I_{res}$  from the distorted image  $I_{dis}$  with the L1 loss  $\ell_{L1}$  and feature reconstruction loss  $\ell_{feat}$  [31], as follows:

$$L_{ind} = \alpha \cdot \ell_{L1}(I_{res}, I_{ori}) + \beta \cdot \ell_{feat}(I_{res}, I_{ori}), \quad (1)$$

where  $\alpha$  and  $\beta$  are scale factors for each loss function.

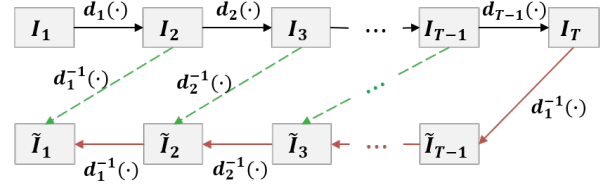


Fig. 4. **Image distort-and-restore process for the collective learning of ISP tools.**  $d_t(\cdot)$  indicates random image distortion function and  $d_t^{-1}(\cdot)$  denotes corresponding image restoration tool. The red-line and green dash-line represents global and local restoration trajectories, respectively.

2) *Collective Tool Training.*: As described in [32], [30], the cascading of two separately trained networks usually cause undesirable unseen artifact. Therefore, we train all network-based tools collectively to relieve the artifact problem in a self-supervised manner. As shown in Fig. 4, the underlying idea is to train the network-based tools to deal with the unseen artifacts without forgetting their pre-learned restore ability. Compared to [30], our collective tool training exploits both global and local restoration trajectories as follows:

$$L_{col} = \epsilon \cdot \ell_{L1}(\tilde{I}_1^G, I_1) + (1 - \epsilon) \cdot \sum_{t=1}^{T-1} \ell_{L1}(\tilde{I}_t^L, I_t), \quad (2)$$

where  $\epsilon$  is a scale factor,  $\tilde{I}_1^G$  indicates the recovered image following the global trajectory, and  $\tilde{I}_t^L$  indicates the recovered image following the local trajectory. Based on the collective tool training, the networks can handle the unseen artifacts while enhancing global restoration and preserving their pre-learned ability with local restoration trajectory.

## V. DRL BASED TOOL SELECTOR

The proposed tool selector consists of a feature extractor  $F$  and a DRL agent, as shown in Fig. 2. At the beginning of each episode, a demosaiced RAW input image  $I_1$  is fed to the tool selector. In each timestep  $t$ , the feature extractor  $F$  extracts the feature vector  $f_t^{ag} = [f_t^i, f_t^g, f_t^s]$ . The policy network  $\pi_\phi$  of the DRL agent chooses a proper action  $a_t \sim \pi(f_t^{ag})$ . The corresponding tool  $a_t$  is applied to the given

image. After that, a processed image  $I_{t+1} = a_t(I_t)$  and a reward  $r_{t+1} = R(I_t, I_{t+1})$  are given. The episode ends when the timestep  $t$  reaches the maximum episode timestep  $T$ , or the STOP action is chosen.

### A. Feature Extractor

In terms of DRL-agent, a well-represented state vector is a key prerequisite to deciding appropriate action. We empirically found that the implicit feature learning network, such as convolutional neural network (CNN), tends to extract less informative feature vector that leads to overall low performance because of spares supervision of reinforcement learning, as validated in Tab. VI-(a). Therefore, we design an explicit feature extraction module that extracts each feature vector from the intensity, gradient, and semantic space of the given image to represent various image properties.

Given input image  $I$  is converted to intensity and gradient image via gray-scale conversion and Sobel operator. After that, we apply the multi-scale histogram method [33] to the intensity and gradient image to extract global and local information. For the semantic feature, we utilize ImageNet pre-trained Alexnet [34]. Then, the state vector is decided by aggregating all feature vectors;  $s_t = f_t^{ag}$ , where  $f_t^{ag}$  is a aggregated feature vector from the intensity  $f^i$ , gradient  $f^g$ , and semantic feature  $f^s$ .

### B. DRL Agent

The network architecture of our DRL agent is similar to original Soft Actor-Critic (SAC) [25], except that we use discrete action space [35]. The DRL agent consists of a twinned Q-network  $Q_\theta$  and a policy network  $\pi_\phi$ , as shown in Fig. 2. All networks take the feature vector  $f^{ag}$  extracted from the feature extractor  $F$ . The twinned Q-network estimates two Q-value  $q_1, q_2$ , and the policy network estimates probabilities for all actions. During the training stage, the smaller Q-value is selected as a Q-value  $Q_\theta(s_t)$  for the training stability. Entire networks are trained based on the policy gradient algorithm, as follows:

$$J_\pi(\phi) = E_{s_t \sim D} [\pi_\phi(s_t) [\kappa \log(\pi_\phi(s_t)) - Q_\theta(s_t)]],$$

$$J_Q(\theta) = E_{(s_t, a_t) \sim D} [\frac{1}{2} (Q_\theta(s_t) - (r(s_t, a_t) + \gamma \pi(s_{t+1}) [Q_\theta(s_{t+1}) - \kappa \log(\pi(s_{t+1}))]))],$$

where  $\gamma$  is a discount factor,  $D$  indicates replay buffer, and  $\kappa$  denotes entropy scale factor.

### C. Reward

A reward function is freely definable according to various purpose without considering differentiability. In this section, we define representative reward functions according to the target application, such as RAW-to-RGB restoration, object detection, and single-view depth estimation. The basic form of reward function is as follows :

$$R(I_t, I_{t-1}) = r_s [M(I_t) - M(I_{t-1})],$$

where  $M(\cdot)$  is a metric function and  $r_s$  is a scaling factor for each metric. Here,  $r_s$  can be a negative value for

TABLE II  
METRIC FUNCTIONS FOR VARIOUS TARGET TASKS. EACH METRIC FUNCTION CAN BE UTILIZED SOLELY AND COMBINED WITH ANOTHER FUNCTION FOR COLLABORATIVE EFFECT.

Task	Metric	Metric function $M(I_t)$
RAW-to-RGB	PSNR	$10 \log_{10} \left( \frac{1.0}{\sqrt{\sum (I_t - I_{gt})^2}} \right)$
	Color	$\sum \ I_t - RGB_{target}\ $
	Intensity	$\sum \ I_t - Gray_{target}\ $
Detection	PR	$\sum_{k=1}^n (w_p \text{Pr}(I_t, I_{gt}) + w_r \text{Re}(I_t, I_{gt}))$
	SOPR	$\sum_{k=1}^n \text{SO}(k) (w_p \text{Pr}(I_t, I_{gt}) + w_r \text{Re}(I_t, I_{gt}))$
Depth	RMSE	$\sqrt{\sum (\text{Depth}(I_t) - \text{Depth}_{gt}(I_{gt}))^2}$
	$\delta_1$	$\delta_1(I_t, I_{gt})$

some metrics. The reward function calculates the difference between the metric values of the previous and current images. The metric functions for various tasks are shown in Tab. II.

1) *RAW-to-RGB Restoration*: The most straight-forward metric for the RAW-to-RGB restoration task is to measure the difference between the restored and the original RGB images. Based on the Ground-Truth(GT) RGB images, the DRL agent can learn proper image modification method that mimics the camera ISP. For this purpose, we use PSNR criteria, a widely used image quality metric. Furthermore, we design non-reference based reward metrics such as desirable color and intensity metrics.

2) *RAW-to-RGB Restoration for Vision Task*: One of the most important feature of our algorithm is that we could define the reward function for various purpose. Therefore, we also validate our proposed framework for object detection and depth estimation tasks. We design each task-specific reward such as Precision-Recall based metric for object detection and RMSE based metric for depth estimation task.

**Object Detection.** We use Mask R-CNN [36] with Resnet-50 as a reference detection model. Usually, the mAP metric is used for evaluating object detection performances. However, since the mAP metric requires multiple images to be calculated, we defined Precision-Recall (PR) and Small Object Precision-Recall (SOPR) metric functions. Both functions are calculated by weighted summation of precision Pr and recall Re values with the given bounding boxes. SOPR metric gives more weight to the small objects that have small bounding box areas below a certain threshold.  $w_p$  and  $w_r$  are scaling factors,  $\text{SO}(k)$  is a multiplication factor for the  $k^{\text{th}}$  object which has 1 or the fixed scalar  $w_{so}$  according to object size.

**Depth Estimation.** We utilize SC-SfMlearner [37] as a reference depth model for single-view depth estimation task. Since the depth evaluation result is directly related to the predicted depth map quality, we adopt the representative depth evaluation metrics RMSE and  $\delta_1$  as our metric functions. We believe another depth evaluation metric and unsupervised image reconstruction loss could be alternatively utilized for the reward metric function.

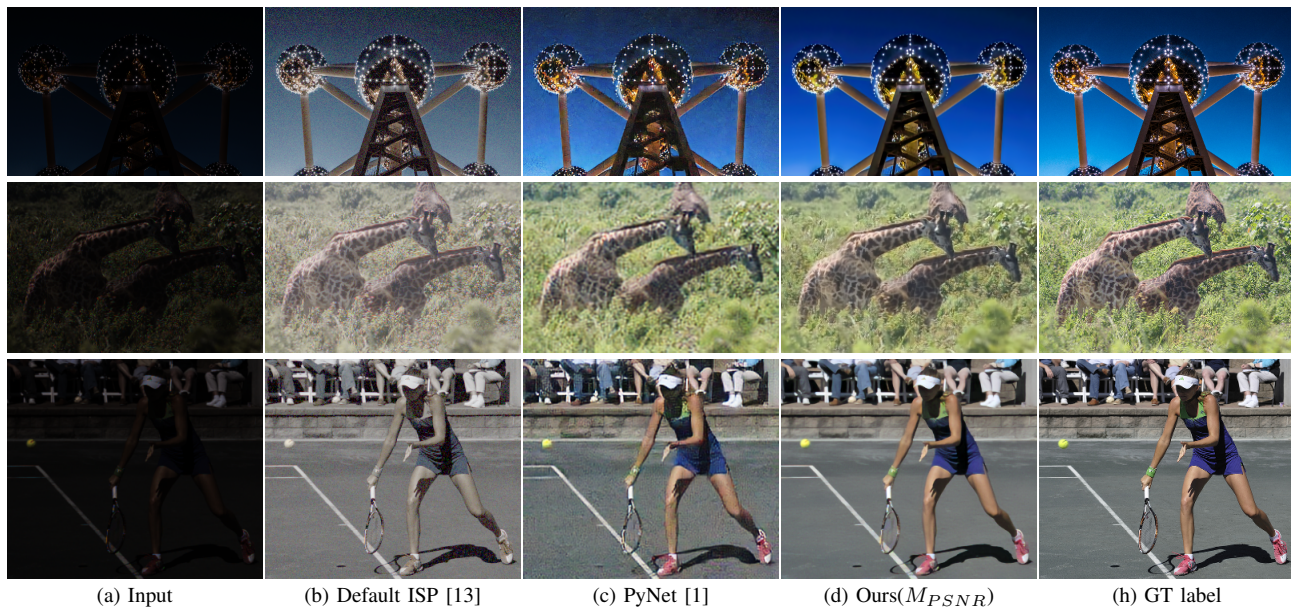


Fig. 5. **Qualitative results for RAW-to-RGB processing task with various reward functions on synthetic datasets.** Ours proposed DRL-ISP framework effectively learns how to process an image according to the given reward function  $M_{PSNR}$ . The proposed framework generates a clean, sharp, and colorful RGB image from the given RAW image by adaptively selecting proper ISP tools.

TABLE III

**QUANTITATIVE RESULTS FOR RAW-TO-RGB PROCESSING TASK. WE TRAIN TOOL SELECTORS ACCORDING TO PSNR REWARD FUNCTION  $M_{PSNR}$  ON THE SYNTHETIC RAW-TO-RGB DATASET.**

Methods	Raw-to-RGB		
	PSNR	SSIM	MSSIM
Default Camera ISP [13]	19.88	0.6540	0.8853
PyNet [1]	23.24	0.7214	0.9246
Ours( $M_{PSNR}$ )	<b>24.82</b>	<b>0.7559</b>	<b>0.9375</b>

## VI. EXPERIMENTAL RESULTS

### A. Implementation Details

**Camera ISP Toolbox.** In order to train CNN-based ISP tools, we construct a dataset that consists of MS-COCO [38], KITTI [39], and DIV2K [40] dataset. For all CNN-based ISP tools except the white-balance tool, we randomly selected 7,000 images from the training set and 1100 images from the testing set. After that, the original images are distorted for the target ISP tool training by adding noise, blur, jpeg compression, resizing, brightness jittering effects, and inverting camera pipeline [41]. The two types of networks (3-layer and 8-layer) are trained with low-level and high-level distortion, respectively. For the white-balance dataset, we utilize the rendered WB dataset(Set2) [6].

**ISP Tool Selector.** We utilizes the above-mentioned ISP toolbox dataset for the DRL agent training. However, the MS-COCO [38], KITTI [39], and DIV2K [40] dataset doesn't provide RAW image. Therefore, firstly, we convert the original RGB image to a RAW Bayer image by utilizing the camera pipeline reversion method [41]. After that, random augmentation such as brightness, noise, and blur effect is added to the converted RAW images to reflect a real-world capturing process. Further details such as hyper-parameter are described in the supplementary video.

### B. RAW-to-RGB Restoration

We train the DRL agent with the camera ISP toolbox and PSNR reward function  $M_{PSNR}$  to investigate the agent can learn how to restore the RGB image from the given RAW image. We compare the trained tool selector with the traditional camera ISP pipeline [13] and high-complexity deep neural network, PyNet [1]. The PyNet is finetuned on the same RAW-to-RGB dataset used for ISP tool selector training during 200 epochs.

The experimental results are quite remarkable in both quantitatively and qualitatively, as shown in Fig. 5 and Tab. III. Even though the tool selector only consists of 2 fully connected layer, the proposed framework effectively generates a clean, sharp, and colorful RGB image from the given image by adaptively selecting proper ISP tools. As shown in Fig. 1-(c), the tool selector processes an image to maximize the reward function step-by-step according to the current image state. Furthermore, by adding a color  $M_{color}$  or intensity  $M_{inten}$  reward, the agent can produces various style of image, as shown in Fig. 6.

### C. RAW-to-RGB for Object Detection

We train tool selectors on the MS-COCO [38] training set with the object detection reward metrics  $M_{PR}$  and  $M_{SOPR}$ . After that, the trained tool selectors are evaluated on the MS-COCO [38] validation set with GT bounding box labels. The experimental results are shown in Fig. 7 and Tab. IV. Interestingly, the tool selectors restore a colorful RGB image from the RAW image without the help of PSNR reward metric  $M_{PSNR}$ . We believe this is because the detection network (*i.e.*, Mask R-CNN) is trained with colorful RGB images (*i.e.*, MS-COCO), the DRL agent tends to produce an image preferred by the detection network. As shown in Tab. IV

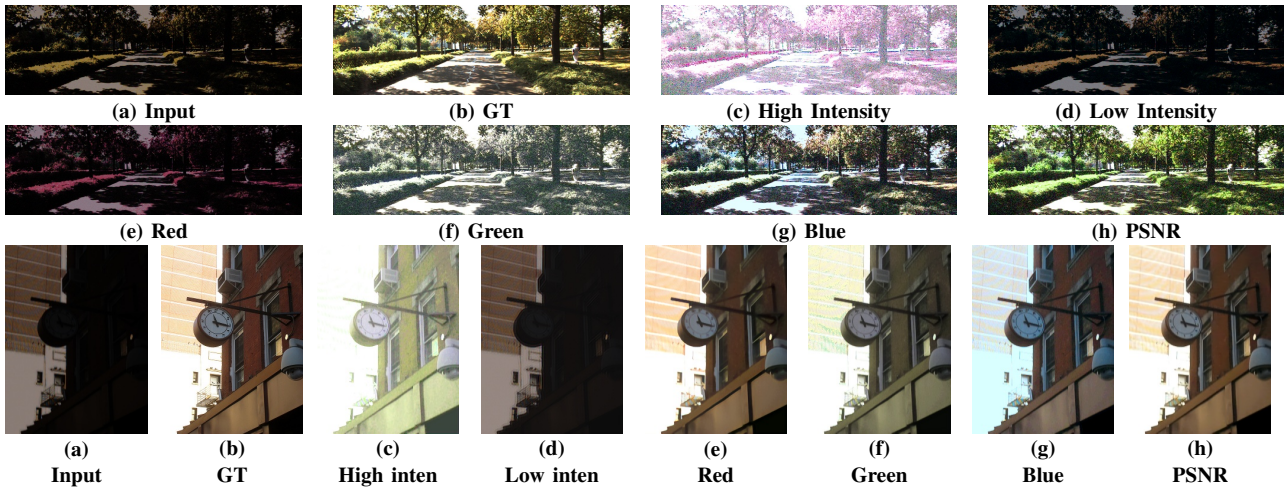


Fig. 6. **Qualitative results for RAW-to-RGB processing task with various reward functions.** (a) Input image, (b) GT, (c) High intensity reward, (d) Low intensity reward, (e) Red reward, (f) Green reward, (g) Blue reward, and (h) PSNR reward. The DRL agent tries to maximize the given reward, therefore, the resulting images show diverse results.

TABLE IV  
QUANTITATIVE RESULTS OF RAW-TO-RGB PROCESSING FOR OBJECT DETECTION TASK ON MS-COCO DATASET [38].

Method	$mAP$	$mAP_{50}$	$mAP_{75}$
Default Camera ISP [13]	24.61	36.85	26.83
Ours( $M_{PR}$ )	23.09	34.88	25.72
Ours( $M_{SOPR}$ )	<b>26.40</b>	<b>39.34</b>	<b>29.48</b>

TABLE V  
QUANTITATIVE RESULTS OF RAW-TO-RGB PROCESSING FOR SINGLE-VIEW DEPTH ESTIMATION TASK ON KITTI DATASET [39].

Methods	Error ↓				Accuracy ↑
	AbsRel	SqRel	RMS	RMSlog	$\delta < 1.25$
Camera ISP [13]	0.131	1.009	5.323	0.210	0.839
Ours( $M_{RMSE}$ )	<b>0.130</b>	<b>0.978</b>	<b>5.220</b>	<b>0.209</b>	<b>0.839</b>
Ours( $M_{\delta_1}$ )	0.155	1.217	5.722	0.238	0.788

and Fig. 7, the small object aware metric  $M_{SOPR}$  shows better detection ability by making DRL-agent produces a small object detail enhanced image.

#### D. RAW-to-RGB for Single-view Depth Estimation

We train tool selectors on the KITTI [39] training set with the depth reward metrics  $M_{RMSE}$  and  $M_{\delta_1}$ . After that, the trained tool selectors are evaluated on the KITTI test set with GT depth labels. The experimental results are shown in Fig. 7 and Tab. V. The tool selectors for the depth estimation task also restore a sharp and colorful image according to depth reward function without the help of PSNR reward metric  $M_{PSNR}$ , same as the object detection task. The results of Tab. V show that the metric  $M_{RMSE}$  performs better than  $M_{\delta_1}$  and default camera ISP. This indicates that some metrics may not be very effective, even if they are directly supervised by the GT labels, and careful reward function designing is essential for better performance improvements.

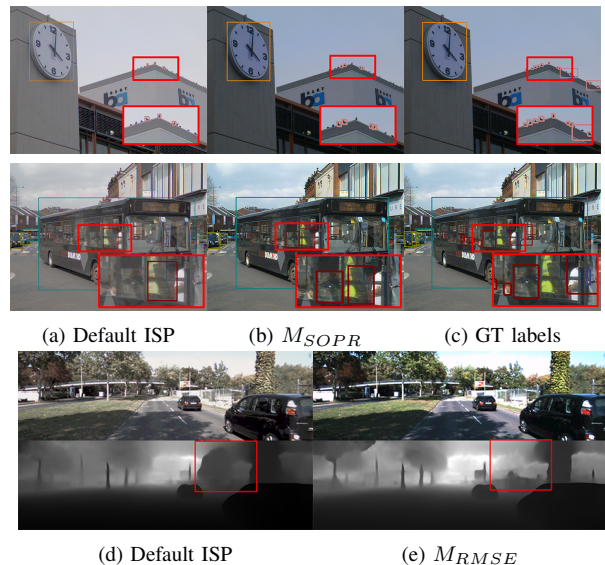


Fig. 7. **Qualitative results of RAW-to-RGB processing for object detection and depth estimation task.** Our tool selector efficiently processes an input image to maximize given reward with respect to the target task.

#### E. Ablation Study

1) *Network Architecture of Tool Selector:* In this ablation study, we investigate the effectiveness of the proposed tool selector structure. The proposed tool selector consists of the feature extractor and the DRL agent. The feature extractor exploits the deterministic feature extraction process from the intensity-, gradient-, and semantic-level. The experimental results are shown in Tab. VI-(a). We also compared our feature extraction methods with the DQN network [42] that has learnable parameters and random fixed parameters [43]. By adding each branch that represents different image properties, the PSNR performance is monotonically increasing. This phenomenon can be interpreted as each feature vector makes a more explicit relation between the state  $s_t$  and action space. For example, the gradient feature could be helpful for edge-enhancing action such as sharpening and super-resolution.

TABLE VI

**ABLATION STUDY OF THE PROPOSED DRL-ISP FRAMEWORK.** WE PERFORM THOROUGH ABLATION STUDIES ON EACH COMPONENT OF THE PROPOSED DRL-ISP FRAMEWORK, SUCH AS THE ARCHITECTURE OF THE TOOL SELECTOR, REINFORCEMENT LEARNING METHOD, AND CAMERA ISP TOOLBOX. THROUGHOUT THE ABLATION STUDY, WE VALIDATE THE EFFECTIVENESS OF THE PROPOSED DRL-ISP FRAMEWORK.

Type	Method	PSNR	SSIM	MSSSIM
Feature Extractor	$N_{DQN}(\text{learn})$	22.40	0.6737	0.8759
	$N_{DQN}(\text{fixed})$	22.50	0.6818	0.8917
	Intensity $f^i$	23.72	0.7147	0.9057
	Gradient $f^g$	18.87	0.6044	0.7995
	Semantic $f^s$	24.11	0.7147	0.9150
	Inten-Grad $[f^i, f^g]$	24.01	0.7213	0.9130
	Inten-Sem $[f^i, f^s]$	23.50	0.7105	0.9085
	Grad-Sem $[f^g, f^s]$	23.48	0.7004	0.8951
	All $[f^i, f^g, f^s]$	<b>24.82</b>	<b>0.7559</b>	<b>0.9375</b>
	Agent	PolicyNet (4 layer)	23.68	0.7116
PolicyNet (3 layer)		24.46	0.7479	0.9293
PolicyNet (2 layer)		<b>24.82</b>	<b>0.7559</b>	<b>0.9375</b>

(a) Network Architectures of the tool selector.

Feature $F$	RL Method	PSNR	SSIM	MSSSIM
$N_{DQN}(\text{learn})$	DQN	6.84	0.0379	0.1935
All $[f^i, f^g, f^s]$	DQN	10.57	0.3852	0.6286
$N_{DQN}(\text{learn})$	SAC	22.40	0.6737	0.8759
All $[f^i, f^g, f^s]$	SAC	<b>24.82</b>	<b>0.7559</b>	<b>0.9375</b>

(b) Reinforcement Learning Training Methods.

Tool	PSNR	SSIM	MSSSIM
$T_{Trad}$	18.70	0.5849	0.8534
$T_{CNN}$	24.52	0.7439	0.9363
$T_{CNN}(wL_{col})$	24.75	0.7550	0.9323
$T_{CNN}(wL_{col}) + T_{trad}$	<b>24.82</b>	<b>0.7559</b>	<b>0.9375</b>

(c) Camera ISP Toolbox.

The learnable feature extractor  $N_{DQN}(\text{learn})$  continuously changes the given image's state as the training progress that leads to an unstable training and requires more training steps. The recent work [43] also supports this claim by showing that the random initialized and fixed network  $N_{DQN}(\text{fixed})$  performs better than the network  $N_{DQN}(\text{learn})$ . However, we find our explicit state definition  $[f^i, f^g, f^s]$  can make more explainable relation than unknown relation  $N_{DQN}(\text{fixed})$  while showing better experimental results. We also investigate the effect of a policy network with 2, 3, and 4 fully-connected layers. The deeper network does not help increase the performances and hinder the relation learning between the state and actions.

2) *Reinforcement Learning Method:* As shown in Tab. VI(b), even if the same feature extractor  $F$  is given, the agent's performance is highly affected by the reinforcement learning methods. As discussed above, the more efficient exploration-and-exploitation methods [44], [45] can greatly increase the performance.

3) *Camera ISP Toolbox:* The camera ISP toolbox designing is also an essential factor for the overall performance since the toolbox's status decides the tool selector's maximum and general ability. As shown in Tab. VI(c), the traditional tools  $T_{Trad}$  can solely enhance the image quality to some extent. However, the performance improvement is quite limited and is boosted by utilizing CNN-based tools  $T_{CNN}$ . The collective tool training  $L_{col}$  that enables cascading more than two networks also enhances the performance by alleviating the unseen artifact problem. The traditional tools  $T_{Trad}$  are able to fine-tune the image with controllable parameters and give a supplement effect for CNN-based tools  $T_{CNN}(wL_{col})$  that resulting outperformed results. The proposed camera ISP toolbox has easily extendable property. Therefore, we will consider more various ISP tools such as traditional color temperature changing and tone mapping.

## VII. CONCLUSION

In this paper, we propose a novel multi-objective camera ISP framework that utilizes Deep Reinforcement Learning (DRL) and camera ISP toolbox that consist of a simple network-based tools and conventional tools. The proposed ISP toolbox consists of light-weight CNN tools and traditional tools that can represent each block of the default camera ISP pipelines, such as gamma correction, color correction, white balance, sharpening, denoising, and others. We also provide an efficient DRL network architecture that can extract the various aspects of an image and make rigid mapping relations between image state and a large number of actions. Our proposed DRL-ISP framework effectively improves the image quality according to various vision tasks such as RAW-to-RGB image restoration, 2D object detection, and monocular depth estimation. Furthermore, our framework can generate various styles of images by freely designing reward functions. For the future works, we plan to apply our DRL-ISP to our vehicle platforms [46], [47] and extend our DRL-ISP to include automatic exposure parameter control [48]. More visual results are available at <https://sites.google.com/view/drl-isp>.

## REFERENCES

- [1] A. Ignatov, L. Van Gool, and R. Timofte, "Replacing mobile camera isp with a single deep learning model," in *Proceedings of the IEEE/CVF Conference on Computer Vision and Pattern Recognition Workshops*, 2020, pp. 536–537.
- [2] E. Schwartz, R. Giryes, and A. M. Bronstein, "Deepisp: Toward learning an end-to-end image processing pipeline," *IEEE Transactions on Image Processing*, vol. 28, no. 2, pp. 912–923, 2018.
- [3] K. Zhang, W. Zuo, Y. Chen, D. Meng, and L. Zhang, "Beyond a gaussian denoiser: Residual learning of deep cnn for image denoising," *IEEE transactions on image processing*, vol. 26, no. 7, pp. 3142–3155, 2017.
- [4] J. Kim, J. Kwon Lee, and K. Mu Lee, "Accurate image super-resolution using very deep convolutional networks," in *Proceedings of the IEEE conference on computer vision and pattern recognition*, 2016, pp. 1646–1654.
- [5] T. Tong, G. Li, X. Liu, and Q. Gao, "Image super-resolution using dense skip connections," in *Proceedings of the IEEE international conference on computer vision*, 2017, pp. 4799–4807.

- [6] M. Afifi, B. Price, S. Cohen, and M. S. Brown, "When color constancy goes wrong: Correcting improperly white-balanced images," in *Proceedings of the IEEE/CVF Conference on Computer Vision and Pattern Recognition*, 2019, pp. 1535–1544.
- [7] M. Afifi and M. S. Brown, "Deep white-balance editing," in *Proceedings of the IEEE/CVF Conference on Computer Vision and Pattern Recognition*, 2020, pp. 1397–1406.
- [8] Y.-L. Liu, W.-S. Lai, Y.-S. Chen, Y.-L. Kao, M.-H. Yang, Y.-Y. Chuang, and J.-B. Huang, "Single-image hdr reconstruction by learning to reverse the camera pipeline," in *Proceedings of the IEEE/CVF Conference on Computer Vision and Pattern Recognition*, 2020, pp. 1651–1660.
- [9] D. Marnierides, T. Bashford-Rogers, J. Hatchett, and K. Debatista, "Expandnet: A deep convolutional neural network for high dynamic range expansion from low dynamic range content," in *Computer Graphics Forum*, vol. 37, no. 2. Wiley Online Library, 2018, pp. 37–49.
- [10] M. Afifi, K. G. Derpanis, B. Ommer, and M. S. Brown, "Learning to correct overexposed and underexposed photos," *arXiv preprint arXiv:2003.11596*, 2020.
- [11] Y. Hu, H. He, C. Xu, B. Wang, and S. Lin, "Exposure: A white-box photo post-processing framework," *ACM Transactions on Graphics (TOG)*, vol. 37, no. 2, pp. 1–17, 2018.
- [12] R. Yu, W. Liu, Y. Zhang, Z. Qu, D. Zhao, and B. Zhang, "Deepexposure: Learning to expose photos with asynchronously reinforced adversarial learning," in *Proceedings of the 32nd International Conference on Neural Information Processing Systems*, 2018, pp. 2153–2163.
- [13] A. Abdelhamed, S. Lin, and M. S. Brown, "A high-quality denoising dataset for smartphone cameras," in *Proceedings of the IEEE Conference on Computer Vision and Pattern Recognition*, 2018, pp. 1692–1700.
- [14] J. Nishimura, T. Gerasimow, R. Sushma, A. Sutic, C.-T. Wu, and G. Michael, "Automatic isp image quality tuning using nonlinear optimization," in *2018 25th IEEE International Conference on Image Processing (ICIP)*. IEEE, 2018, pp. 2471–2475.
- [15] E. Tseng, F. Yu, Y. Yang, F. Mannan, K. S. Arnaud, D. Nowrouzezahrai, J.-F. Lalonde, and F. Heide, "Hyperparameter optimization in black-box image processing using differentiable proxies," *ACM Trans. Graph.*, vol. 38, no. 4, pp. 27–1, 2019.
- [16] L. Yahiaoui, C. Hughes, J. Horgan, B. Deegan, P. Denny, and S. Yogamani, "Optimization of isp parameters for object detection algorithms," *Electronic Imaging*, vol. 2019, no. 15, pp. 44–1, 2019.
- [17] J. Dong, I. Frosio, and J. Kautz, "Learning adaptive parameter tuning for image processing," *Electronic Imaging*, vol. 2018, no. 13, pp. 196–1, 2018.
- [18] L. V. Hevia, M. A. Patricio, J. M. Molina, and A. Berlanga, "Optimization of the isp parameters of a camera through differential evolution," *IEEE Access*, vol. 8, pp. 143 479–143 493, 2020.
- [19] A. Mosleh, A. Sharma, E. Onzon, F. Mannan, N. Robidoux, and F. Heide, "Hardware-in-the-loop end-to-end optimization of camera image processing pipelines," in *Proceedings of the IEEE/CVF Conference on Computer Vision and Pattern Recognition*, 2020, pp. 7529–7538.
- [20] C. Yang, J. Kim, J. Lee, Y. Kim, S.-S. Kim, T. Kim, and J. Yim, "Effective isp tuning framework based on user preference feedback," *Electronic Imaging*, vol. 2020, no. 9, pp. 316–1, 2020.
- [21] M. Buckler, S. Jayasuriya, and A. Sampson, "Reconfiguring the imaging pipeline for computer vision," in *Proceedings of the IEEE International Conference on Computer Vision*, 2017, pp. 975–984.
- [22] C. Chen, Q. Chen, J. Xu, and V. Koltun, "Learning to see in the dark," in *Proceedings of the IEEE Conference on Computer Vision and Pattern Recognition*, 2018, pp. 3291–3300.
- [23] Z. Liang, J. Cai, Z. Cao, and L. Zhang, "Cameranet: A two-stage framework for effective camera isp learning," *IEEE Transactions on Image Processing*, vol. 30, pp. 2248–2262, 2021.
- [24] L. Dai, X. Liu, C. Li, and J. Chen, "Awnet: Attentive wavelet network for image isp," *arXiv preprint arXiv:2008.09228*, 2020.
- [25] T. Haamoja, A. Zhou, P. Abbeel, and S. Levine, "Soft actor-critic: Off-policy maximum entropy deep reinforcement learning with a stochastic actor," in *International Conference on Machine Learning*. PMLR, 2018, pp. 1861–1870.
- [26] A. M. Reza, "Realization of the contrast limited adaptive histogram equalization (clahe) for real-time image enhancement," *Journal of VLSI signal processing systems for signal, image and video technology*, vol. 38, no. 1, pp. 35–44, 2004.
- [27] M. Ebner, *Color constancy*. John Wiley & Sons, 2007, vol. 7.
- [28] G. Bradski and A. Kaehler, *Learning OpenCV: Computer vision with the OpenCV library*. O'Reilly Media, Inc., 2008.
- [29] E. Riba, D. Mishkin, D. Ponsa, E. Rublee, and G. Bradski, "Kornia: an open source differentiable computer vision library for pytorch," in *Proceedings of the IEEE/CVF Winter Conference on Applications of Computer Vision*, 2020, pp. 3674–3683.
- [30] K. Yu, C. Dong, L. Lin, and C. Change Loy, "Crafting a toolchain for image restoration by deep reinforcement learning," in *Proceedings of the IEEE conference on computer vision and pattern recognition*, 2018, pp. 2443–2452.
- [31] J. Johnson, A. Alahi, and L. Fei-Fei, "Perceptual losses for real-time style transfer and super-resolution," in *European conference on computer vision*. Springer, 2016, pp. 694–711.
- [32] K. Zhang, W. Zuo, and L. Zhang, "Deep plug-and-play super-resolution for arbitrary blur kernels," in *Proceedings of the IEEE/CVF Conference on Computer Vision and Pattern Recognition*, 2019, pp. 1671–1681.
- [33] Z. Wang, J. Zhang, M. Lin, J. Wang, P. Luo, and J. Ren, "Learning a reinforced agent for flexible exposure bracketing selection," in *Proceedings of the IEEE/CVF Conference on Computer Vision and Pattern Recognition*, 2020, pp. 1820–1828.
- [34] A. Krizhevsky, I. Sutskever, and G. E. Hinton, "Imagenet classification with deep convolutional neural networks," *Advances in neural information processing systems*, vol. 25, pp. 1097–1105, 2012.
- [35] P. Christodoulou, "Soft actor-critic for discrete action settings," *arXiv preprint arXiv:1910.07207*, 2019.
- [36] K. He, G. Gkioxari, P. Dollár, and R. Girshick, "Mask r-cnn," in *Proceedings of the IEEE international conference on computer vision*, 2017, pp. 2961–2969.
- [37] J.-W. Bian, Z. Li, N. Wang, H. Zhan, C. Shen, M.-M. Cheng, and I. Reid, "Unsupervised scale-consistent depth and ego-motion learning from monocular video," *arXiv preprint arXiv:1908.10553*, 2019.
- [38] T.-Y. Lin, M. Maire, S. Belongie, J. Hays, P. Perona, D. Ramanan, P. Dollár, and C. L. Zitnick, "Microsoft coco: Common objects in context," in *European conference on computer vision*. Springer, 2014, pp. 740–755.
- [39] A. Geiger, P. Lenz, and R. Urtasun, "Are we ready for autonomous driving? the kitti vision benchmark suite," in *2012 IEEE Conference on Computer Vision and Pattern Recognition*. IEEE, 2012, pp. 3354–3361.
- [40] E. Agustsson and R. Timofte, "Ntire 2017 challenge on single image super-resolution: Dataset and study," in *The IEEE Conference on Computer Vision and Pattern Recognition (CVPR) Workshops*, July 2017.
- [41] M. Buckler, S. Jayasuriya, and A. Sampson, "Reconfiguring the imaging pipeline for computer vision," in *The IEEE International Conference on Computer Vision (ICCV)*, 2017.
- [42] V. Mnih, K. Kavukcuoglu, D. Silver, A. A. Rusu, J. Veness, M. G. Bellemare, A. Graves, M. Riedmiller, A. K. Fidjeland, G. Ostrovski, et al., "Human-level control through deep reinforcement learning," *nature*, vol. 518, no. 7540, pp. 529–533, 2015.
- [43] Y. Seo, L. Chen, J. Shin, H. Lee, P. Abbeel, and K. Lee, "State entropy maximization with random encoders for efficient exploration," *arXiv preprint arXiv:2102.09430*, 2021.
- [44] T. Schaul, J. Quan, I. Antonoglou, and D. Silver, "Prioritized experience replay," *arXiv preprint arXiv:1511.05952*, 2015.
- [45] K. Lee, B. Lee, U. Shin, and I.-S. Kweon, "An efficient asynchronous method for integrating evolutionary and gradient-based policy search," in *34th Conference on Neural Information Processing Systems, NeurIPS 2020*. Conference on Neural Information Processing Systems, 2020.
- [46] J. Park, U. Shin, G. Shim, K. Joo, F. Rameau, J. Kim, D.-G. Choi, and I. S. Kweon, "Vehicular multi-camera sensor system for automated visual inspection of electric power distribution equipment," in *2019 IEEE/RSJ International Conference on Intelligent Robots and Systems (IROS)*. IEEE, 2019, pp. 281–288.
- [47] F. Rameau, O. Bailo, J. Park, K. Joo, and I. S. Kweon, "Real-time multi-car localization and see-through system," *International Journal of Computer Vision*, vol. 130, no. 2, pp. 384–404, 2022.
- [48] U. Shin, J. Park, G. Shim, F. Rameau, and I. S. Kweon, "Camera exposure control for robust robot vision with noise-aware image quality assessment," in *2019 IEEE/RSJ International Conference on Intelligent Robots and Systems (IROS)*. IEEE, 2019, pp. 1165–1172.